RESEARCH ARTICLE

Editor's Choice

NANO · MICRO small

www.small-journal.com

Ultrasmall 2D Sn-Doped $MAPbBr_3$ Nanoplatelets Enable Bright Pure-Blue Emission

*Fengjun Chun, Kyung Yeon Jang, Huanyu Zhou, Sungjin Kim, Eojin Yoon, and Tae-Woo Lee**

Synthesis of perovskites that exhibit pure-blue emission with high photoluminescence quantum yield (PLQY) in both nanocrystal solutions and nanocrystal-only films presents a significant challenge. In this work, a room-temperature method is developed to synthesize ultrasmall, monodispersed, Sn-doped methylammonium lead bromide ($MAPb_{1-x}Sn_xBr_3$) perovskite nanoplatelets (NPLs) in which the strong quantum confinement effect endows pure blue emission (460 nm) and a high quantum yield (87%). Post-treatment using n-hexylammonium bromide (HABr) repaired surface defects and thus substantially increased the stability and PLQY (80%) of the NPL films. Concurrently, high-precision patterned films (200-µm linewidth) are successfully fabricated by using cost-effective spray-coating technology. This research provides a novel perspective for the preparation of high PLQY, highly stable, and easily processable perovskite nanomaterials.

1. Introduction

Solution-processable metal halide perovskites (MHPs) are rapidly advancing as potential candidates for optoelectronics, primarily due to their remarkable properties such as tunable bandgap, narrow emission spectra, high photoluminescent quantum yield (PLQY) and cost-effectiveness.[1–4] Use of MHPs has yielded substantial advances in various optoelectronic applications. Despite concerted efforts toward the development of blue-emitting perovskites, these remain substantially behind their green and red counterparts.[5,6] The introduction of chlorine into bromine-based perovskites as a means of tuning the bandgap provides a convenient route to blue emission perovskites. Nonetheless, halide segregation induced by halide ion migration is an inescapable consequence of mixed-halide perovskites, rendering pure bromine-based perovskites with quantum confinement effects a highly viable strategy.[7–14]

Size confinement and dimensional control are the main strategies for pure bromine-based perovskites to emit blue light. The necessity for a band gap in the blue spectral region demands nanoparticles that are smaller than the Bohr exciton diameter; this requirement poses a challenge because colloidal nanoparticles synthesized using current methods are unstable and inherent polydispersed.[15] Quantum-confined 0D pure bromine-based perovskite quantum dots with pure blue emission (≤470 nm) have been achieved.[16,17] However, pure-blue emission with narrow full width at half maximum (FWHM) is difficult to obtain because of the wide size distribution and strongly size-dependent emission.[18–21] Use of 2D pure bromide-based perovskite nanoplatelets (NPLs) is an alternative way to achieve blue emission with a narrow FWHM due to their quantized thickness[22] however, the intricate process of nucleation and lattice construction tends to introduce significant surface defects, which cause noticeable band tails and a relatively low PLQY. Additionally, the uncontrollable distribution of n-monolayers also hinders the further development of 2D perovskite.[23,24]

Moreover, high PLQY of perovskite nanoparticles solution is seldom effectively reproduced in spin-coated solid films, which typically have extremely low PLQY (<30–40%) without passivation.[25–27] This phenomenon may occur because effective passivation in solution is not replicated when the surface is directly exposed to oxygen, moisture, or environmental pollutants.[28,29] Additionally, the increased density of packing in films can facilitate energy transfer to trap states and augment self-absorption. Consequently, the fabrication of perovskite nanoparticle films often necessitates an inert environment, like a glove box, or embedding the nanocrystals in insulating polymers to enhance their stability and quantum yield. To meet the

F. Chun, K. Y. Jang, H. Zhou, S. Kim, E. Yoon, T.-W. Lee
Department of Materials Science and Engineering
Seoul National University
1 Gwanak-ro, Gwanak-gu, Seoul 08826, Republic of Korea
E-mail: twlees@snu.ac.kr

H. Zhou
BK21 PLUS SNU Materials Division for Educating Creative Global Leaders
Seoul National University
Seoul 08826, Republic of Korea

T.-W. Lee
Institute of Engineering Research, Research Institute of Advanced Materials, Soft Foundry
Seoul National University
Seoul 08826, Republic of Korea

T.-W. Lee
SN Display Co., Ltd.
Seoul 08826, Republic of Korea

DOI: 10.1002/smll.202400959

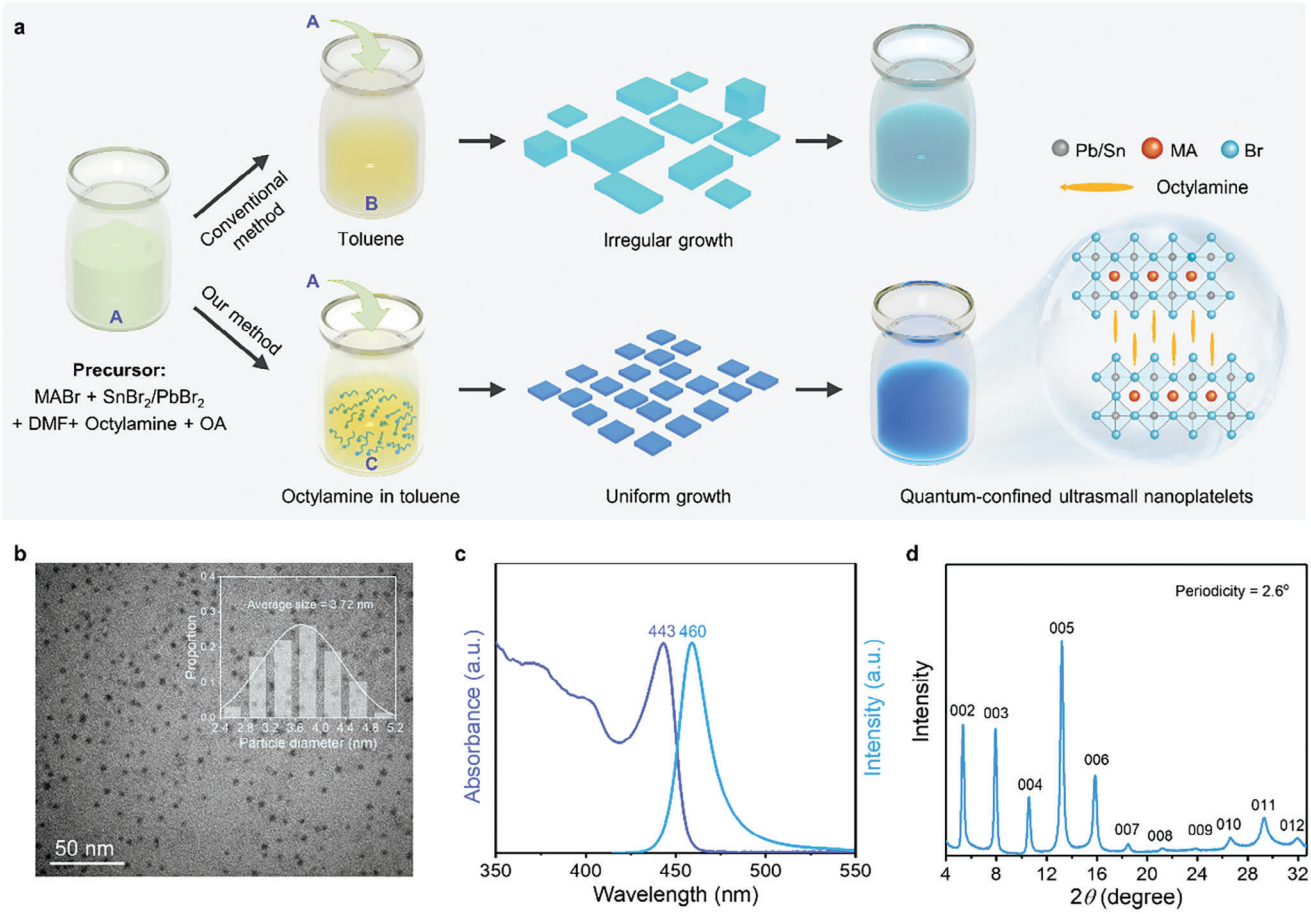

Figure 1. Synthesis and characterization of blue-emitting ultrasmall Sn-doped $MAPbBr_3$ NPLs. a) Schematic illustration of the synthesis procedure. b) TEM image (inset: size distribution). c) Absorption and PL spectra. d) XRD pattern.

needs of large-scale applications, the development of long-term stable materials that maintain high PLQY in films, akin to that in solution, is of pressing need.

Here, we report a room-temperature method to synthesize ultrasmall (≈3.7 nm) $MAPb_{1-x}Sn_xBr_3$ NPLs that exhibit pure-blue emission, which was achieved by immediately suppressing rapid crystal nucleation and growth. The strong quantum confinement of the monodispersed ultrasmall NPLs enables bright blue emission at 460 nm with a narrow FWHM of 20 nm. Partial substitution of the toxic Pb^{2+} with Sn^{2+} not only mitigates toxicity but also significantly enhances PL performance. The use of n-hexylammonium bromide (HABr) as a passivating compound decreased non-radiative recombination loss both in NPL solution and solid film, thereby achieving a PLQY of 87% in solution and 80% in film. Furthermore, NPL solution can be spray-coated directly on various substrates without the addition of polymers. This easily scalable film-forming technology presents significant potential for large-scale applications and achieving high-precision patterning.

2. Results and Discussion

Ultrasmall $MAPb_{1-x}Sn_xBr_3$ NPLs were synthesized at room temperature using a modified ligand-assisted reprecipitation (LARP) method (**Figure** 1a). The precursor solution was formulated by solubilizing methylammonium bromide (MABr), a mixture of lead bromide ($PbBr_2$) and tin bromide ($SnBr_2$), oleic acid (OA), along with octylamine (OCT) in N, N-dimethylformamide (DMF). Unlike conventional procedure in LARP, a specific amount of OCT was pre-introduced to the anti-solvent (toluene) and thoroughly mixed: the OCT in toluene suppresses the growth of $MAPb_{1-x}Sn_xBr_3$ crystals and prevents the formation of irregular particles that emit mixed-wavelength light. The precursor solution was slowly injected into the anti-solvent mixture under vigorous stirring, leading to the formation of a pure blue-emitting crude solution. Transmission electron microscopy (TEM) analysis of the $MAPb_{0.6}Sn_{0.4}Br_3$ NPLs revealed that they were monodispersed, with an average diameter of ≈3.7 nm (Figure 1b). The narrow size distribution and high monodispersity were further confirmed by scanning transmission electron microscopy (STEM) images, as shown in Figure S1 (Supporting Information). For comparison, $MAPbBr_3$ was also synthesized by introducing OCT only, either to the precursor or the anti-solvent; the resulting $MAPbBr_3$ had a broad distribution of size and shape, and did not emit pure blue light (Table S1 and Figure S2, Supporting Information). Amine ligands are critical in the synthesis and stabilization of perovskite nanoparticles, and the PL emission can be tuned by adjusting the OCT

concentration in the precursor.[30] In a control experiment, we progressively increased the amount of OCT in the precursor used to synthesize $MAPbBr_3$ (Figure S3, Supporting Information). As the OCT volume increased, the quantum confinement effect in the lateral direction strengthened, which caused the PL spectrum to shift from green to cyan and then to blue. This shift is attributed to the formation of 2D platelets (Figure S4a, Supporting Information). Our results suggest that achieving deep blue emission with high color purity requires quantum confinement in both the vertical and horizontal directions.

In this modified process, OCT is used in both the precursor and the antisolvent, diverging from the conventional LARP method where OCT is limited to the precursor. During the reaction process, OCT is partially protonated to OCT^+, which subsequently interacts with the inorganic frameworks of the perovskite via hydrogen bonding. The residual OCT and OA serve as ligands, which manage nucleation and growth, thereby facilitating the construction of ultrasmall 2D NPLs with pure-blue emission. The morphology and size of the NPLs can be controlled by pre-introducing an appropriate amount of OCT into the antisolvent, preventing the formation of large sheet-like structures and broad emission (Figures S4b, S5, Supporting Information). Furthermore, the homogeneous distribution of OCT in the antisolvent helps to passivate surface defects, thus helping to increase the PLQY.

As illustrated in Figure 1c, the dominant and strong excitonic peak at 443 nm, in conjunction with a single PL emission peak at 460 nm, confirms the formation of 2D NPLs. Both peaks matched well with those of n = 3 NPLs.[31,32] $MAPb_{0.6}Sn_{0.4}Br_3$ NPLs have a 2D multilayered configuration that assembles by insertion of the long-chain organic cation (OCT^+). The XRD pattern (Figure 1d) shows pronounced periodic diffraction peaks at low angles, suggesting NPLs stacking. The clear periodic 2D crystallographic planes (00k) reveal preferential orientation and high phase purity. Applying Bragg's law, the average interlayer spacing of the NPLs was calculated to be ≈3.4 nm, aligning with the cumulative thickness of n = 3 layered perovskites (≈1.8 nm) and two intercalated organic cation layers of 1.6 nm. Atomic force microscopy (AFM) was used to further quantify the thickness of the NPLs, revealing that the thinnest NPLs measured 3.1 nm (Figure S6, Supporting Information). The overestimated thickness can be attributed to the noncontact AFM tapping mode and the presence of surface organic molecules.[32–35]

The crude solution prepared by this method progressively begins to show turbidity after 15 minutes of storage, and its PLQY markedly diminishes (Figure S7, Supporting Information). To improve the stability, an equal volume of acetonitrile was introduced into the crude solution, which facilitated the purification of the 2D $MAPb_{1-x}Sn_xBr_3$ NPLs. This process imparted high stability to the $MAPb_{0.6}Sn_{0.4}Br_3$ NPLs even after exposure to air for a month (Figure S8, Supporting Information), making them suitable for further applications. After optimizing a series of reaction conditions (Figures S9–S12, Supporting Information), the NPLs demonstrated high PLQY (80%) and long-term ambient storage stability.

A series of purified $MAPb_{1-x}Sn_xBr_3$ NPLs were prepared using the same method. The PL emission spectra of $MAPb_{0.6}Sn_{0.4}Br_3$ NPLs showed a slight redshift in comparison to undoped $MAPbBr_3$ NPLs, which corresponds well with the absorption spectra (**Figure 2a**). This shift can be attributed to the reduction of the bandgap from 2.8 eV in $MAPbBr_3$ NPLs to 2.75 eV in $MAPb_{0.6}Sn_{0.4}Br_3$ NPLs, as calculated from the absorption spectra by using a Tauc plot (Figure S13, Supporting Information). This decrease in bandgap can be attributed to the smaller ionic radius and higher electronegativity of the Sn^{2+} ions compared to Pb^{2+} ions; these differences induce lattice contraction and increase the overlap of the p orbital of the B-site metal with that of the halogen.[36,37]

The doping concentration of Sn^{2+} influenced the PL of the $MAPb_{1-x}Sn_xBr_3$ NPLs. As the concentration of Sn^{2+} increased, the PL emission peaks exhibited a gradual red shift (Figure 2d), and the PLQY initially increased and then decreased (Figure 2e). The PLQY increased from 37% in undoped NPLs to 80% in NPLs with $x = 0.4$; this change affirms the positive influence of Sn^{2+} ions. This enhancement is likely due to a reduction in carrier trapping states, with doping promoting the efficient utilization of excited carriers.[38,39] To further understand the mechanism behind the PLQY enhancement caused by Sn^{2+} doping, TRPL measurements were conducted (Figure 2c). The average PL lifetime for $MAPb_{0.6}Sn_{0.4}Br_3$ NPLs (15.33 ns) exceeds that of the undoped counterparts (6.14 ns), suggesting that the presence of Sn^{2+} expands the radiative recombination channel.[40] In the XRD spectra, the diffraction peak shifted to larger angles upon the introduction of Sn, indicating the successful formation of $MAPb_{1-x}Sn_xBr_3$ NPLs (Figure 2b). Notably, doping with other ions also positively impacted the enhancement of PLQY, but doping with Sn^{2+} yielded NPLs that had the highest PLQY (Figure 2f).

Although purified $MAPb_{0.6}Sn_{0.4}Br_3$ NPL solution demonstrated high PLQY, fabricating NPL films that also had high PLQY proved to be challenging. After the NPL solution was spin-coated on glass substrates, the PLQY dropped from 80% to 40% (**Figure 3b**). To engineer NPL films with high PLQY, numerous bromide-containing organic cations (R-Br, R = n-butylammonium (BA), n-hexylammonium (HA), n-octylammonium (OA), phenylammonium (PhA), benzylammonium (BZA)) were utilized to passivate the perovskite surface via a post-treatment process. A certain amount of R-Br was dissolved in toluene and used to disperse the purified $MAPb_{0.6}Sn_{0.4}Br_3$ NPLs. The various R-Br passivated $MAPb_{0.6}Sn_{0.4}Br_3$ solution and films achieved varying PLQYs, with these variations primarily attributed to differences in the chain lengths of R-Br and their differing solubilities in toluene (Figure S14, Supporting Information). Figure S14c (Supporting Information) demonstrates that OABr and HABr have greater solubility in toluene, therefore, their introduction has played a positive role in improving the PLQY. The comparatively abbreviated chain length of HABr facilitates more compact molecular arrangement on the surface of the NPLs, attributable to diminished steric hindrance, thereby engendering a more effective passivation effect.

Following post-treatment with HABr, Br^- in solution was attracted to Br-vacancy positions of the octahedron and anchored there, thereby decreasing the number of trap states and increasing the PLQY (Figure 3a). The HABr-passivated NPLs demonstrate enhanced PLQY compared with previous reports, recording 87% in solution and 80% in film format, attributable to the repair of surface defects (Figure 3c and Table S2, Supporting Information). TRPL measurements demonstrated that passivation of the $MAPb_{0.6}Sn_{0.4}Br_3$ NPLs extended their average lifetime to

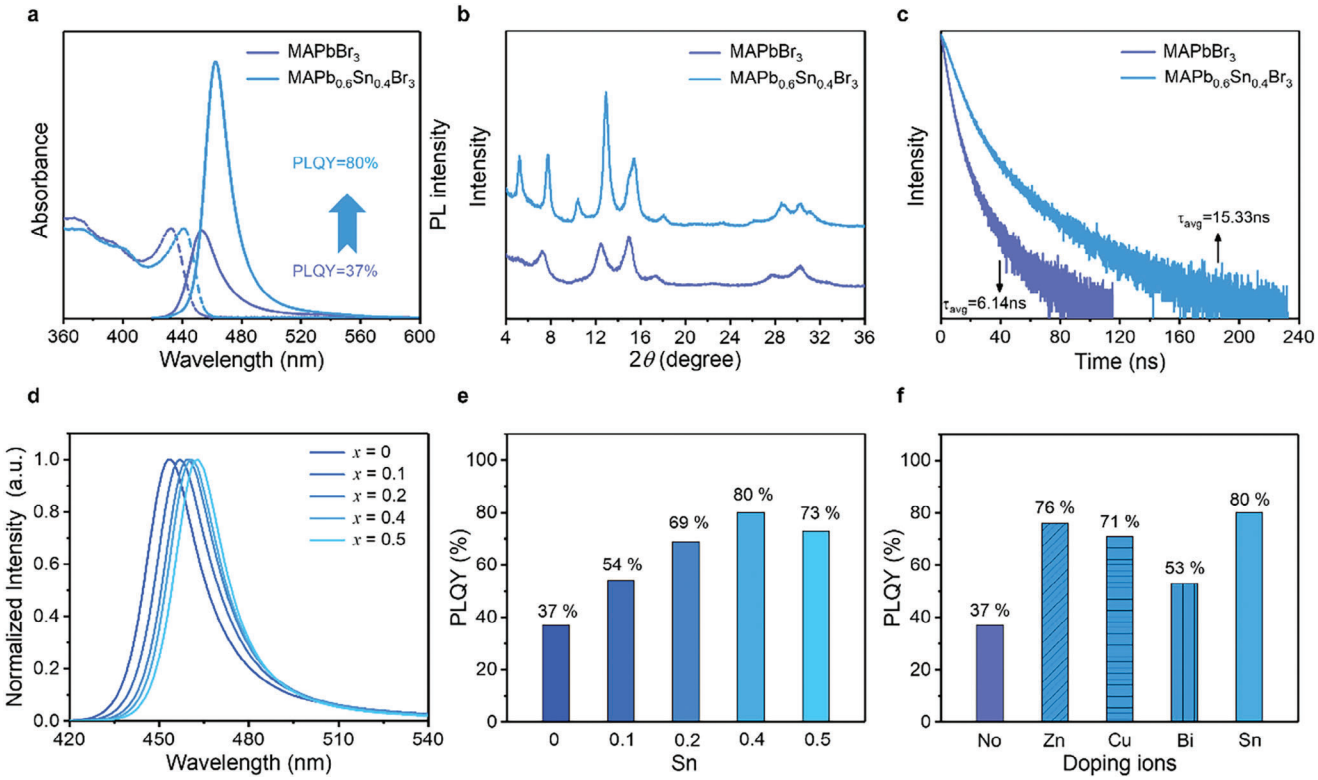

Figure 2. Optical and structural properties of $MAPb_{1-x}Sn_xBr_3$ NPLs. a) Absorption and PL spectra of un-doped $MAPbBr_3$ and $MAPb_{0.6}Sn_{0.4}Br_3$ NPLs. b) XRD pattern of un-doped $MAPbBr_3$ and $MAPb_{0.6}Sn_{0.4}Br_3$ NPLs. c) Time-resolved PL decay of un-doped $MAPbBr_3$ and $MAPb_{0.6}Sn_{0.4}Br_3$ NPLs. d) Normalized PL spectra of $MAPb_{1-x}Sn_xBr_3$ NPLs. e) Relative PLQY of $MAPb_{1-x}Sn_xBr_3$ NPLs. f) PLQY comparison for $MAPbBr_3$ NPLs doped with different metal ions.

26.57 ns, indicating that HABr passivation effectively reduces nonradiative carrier recombination (Figure 3d). Conversely, the increased trap states at the interface of the un-passivated NPL film augmented the non-radiative recombination of excitons, resulting in a shortened lifetime. Furthermore, the XRD pattern indicates that the $MAPb_{0.6}Sn_{0.4}Br_3$ NPLs retain their 2D structure after HABr treatment (Figure S15, Supporting Information).

X-ray photoelectron spectroscopy (XPS) analysis (Figure 3e–g) was conducted to examine the elemental composition of both unpassivated and HABr-passivated $MAPb_{0.6}Sn_{0.4}Br_3$ NPL films. The XPS spectra of Pb (Figure 3e) showed primary peaks with high binding energies, which were attributed to the $4f_{5/2}$ and $4f_{7/2}$ states of divalent Pb^{2+}, and shoulder peaks at relatively low binding energies that were ascribed to metallic Pb^0. For the unpassivated NPLs, the surface uncoordinated Pb^{2+} ion can convert to Pb^0 by light or X-ray irradiation, inducing non-radiative recombination acting as recombination center.[41] Comparatively, the signal of metallic Pb^0 was significantly weaker after passivation using HABr, indicating that the repair of Br vacancies on the NPLs surface terminated the conversion of Pb^{2+} to Pb^0. The XPS spectra of Sn (Figure 3f) showed conspicuous Sn 3d peaks; their presence indicates successful incorporation of Sn atoms into $MAPbBr_3$ NPLs. Some Sn^{2+} was oxidized to Sn^{4+}, but Sn^{2+} remained the dominant Sn species. This high stability of Sn^{2+} is unlike conventional Sn-based perovskites, which have poor ambient stability because Sn^{2+} readily oxidizes. This difference occurs because the NPLs have 2D structure and high ligand density, which together efficiently suppress external oxidation. The XPS spectra of Br (Figure 3g) showed a broad Br 3d peak, which was deconvoluted into two peaks corresponding to inner and surface Br ions. After passivation, the binding energies of these peaks decreased slightly. This change can be attributed to a decrease in electron density owing to the strong interaction with HABr.[42,43]

Poor stability when exposed to air and humidity is a principal challenge for perovskites, particularly for blue-emitting perovskites. In addition to enhancing the PLQY, we discovered that the stability of $MAPb_{0.6}Sn_{0.4}Br_3$ NPLs was significantly improved after passivation with HABr. The HABr-passivated $MAPb_{0.6}Sn_{0.4}Br_3$ NPLs maintained high monodispersity without noticeable agglomeration after exposure to ambient conditions for 30 days (**Figure** 4a,b). The solution of unpassivated $MAPb_{0.6}Sn_{0.4}Br_3$ NPLs became turbid, and its PLQY decreased to 50% (Figure 4c,d). In contrast, the solution of HABr-passivated $MAPb_{0.6}Sn_{0.4}Br_3$ NPLs remained clear, the emission peak showed a negligible red-shift, and the PLQY showed an insignificant reduction; these results all attest to the superior long-term stability of HABr-passivated $MAPb_{0.6}Sn_{0.4}Br_3$ NPLs (Figure 4c,e). Remarkably, the spin-coated films of HABr-passivated $MAPb_{0.6}Sn_{0.4}Br_3$ NPLs also exhibited improved environmental stability across various temperature and humidity conditions (Figure 4f; Figure S16, Supporting Information), suggesting a variety of potential applications.

Spray coating technology offers a more straightforward approach to achieving cost-effective, large-scale, rapidly scalable,

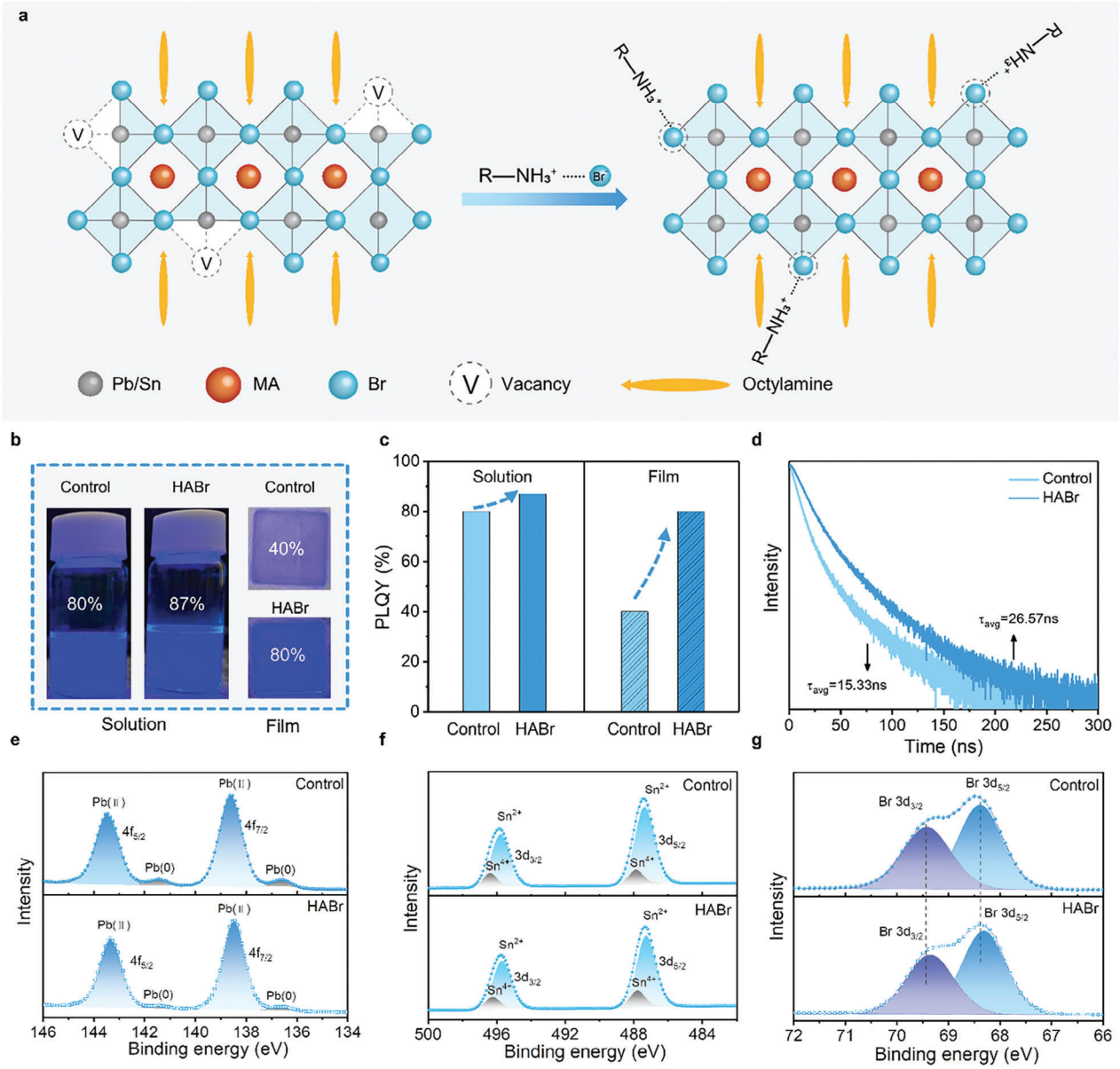

Figure 3. Comparative performance of $MAPb_{0.6}Sn_{0.4}Br_3$ NPLs without passivation (control) and with HABr passivation. a) Schematic representation of the HABr passivation process. b) Photographs of both the solution and films under UV light. c) PLQY of solution and films. d) Time-resolved PL decay curves. e–g) High-resolution XPS spectra of Pb (e), Sn (f), and Br (g) for $MAPb_{0.6}Sn_{0.4}Br_3$ NPLs films.

and patterned thin film deposition. Benefiting from the superior surface wettability, the $MAPb_{0.6}Sn_{0.4}Br_3$ NPL solution, devoid of any binder materials, can be spray-coated directly onto a variety of substrates to form high-precision patterns (Figures S17 and S18, Supporting Information). As depicted in Figure 4g, jellyfish-patterned $MAPb_{0.6}Sn_{0.4}Br_3$ NPL films manifest bright blue emission on these substrates under UV light. The emission spectra (Figure S19, Supporting Information) of films spray-coated with unpassivated NPLs exhibit a shoulder peak in the green region, which is absent in films spray-coated with HABr-passivated NPLs. This indicates that HABr passivation significantly enhances the stability of $MAPb_{0.6}Sn_{0.4}Br_3$ NPLs across different substrates. Furthermore, a highly stretchable butterfly pattern was successfully fabricated by spraying solution of HABr-passivated NPLs directly onto the SEBS substrate (Figure 4h). This stretchable film retained its blue emission without developing green light emission after 30 days of exposure to ambient air, demonstrating good ambient stability (Figure S20, Supporting Information). These attributes highlight the unique benefits of spray coating technology compared to other film deposition techniques.

3. Conclusion

In summary, we synthesized ultrasmall $MAPb_{1-x}Sn_xBr_3$ NPLs using a straightforward room-temperature method that suppresses

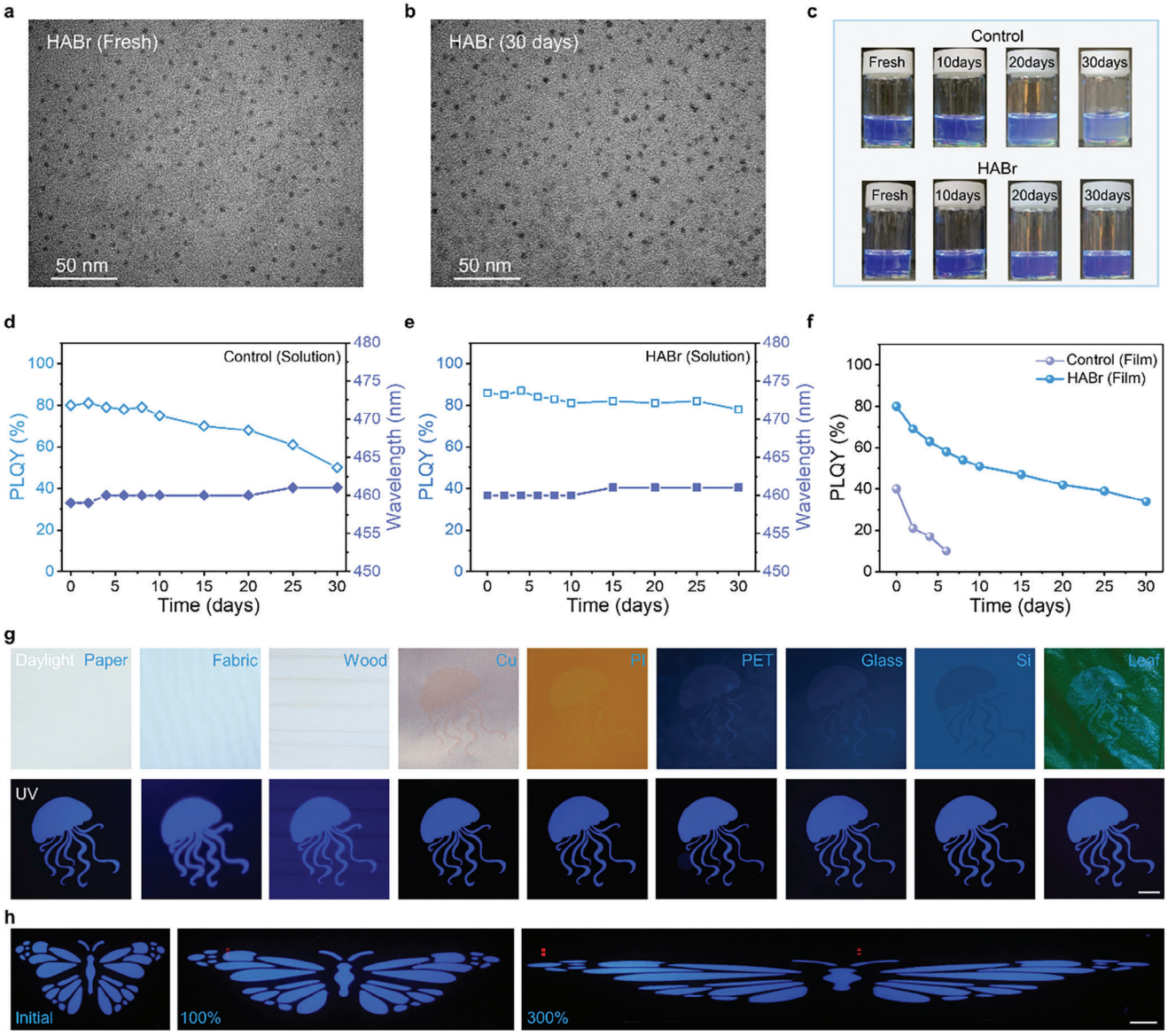

Figure 4. Stability and application of $MAPb_{0.6}Sn_{0.4}Br_3$ NPLs. a,b) TEM images of fresh (a) and 30-day-stored (b) HABr-passivated $MAPb_{0.6}Sn_{0.4}Br_3$ NPLs. c) Photographs of $MAPb_{0.6}Sn_{0.4}Br_3$ NPLs without passivation (control) and with HABr passivation after aging for 0, 10, 20 and 30 days. d,e) Changes in PLQY and peak emission wavelength over time for NPLs without passivation (d) and with HABr passivation (e). f) Long-term stability of $MAPb_{0.6}Sn_{0.4}Br_3$ NPL films (RT, RH = 17%). g) Photographs of patterned HABr passivated $MAPb_{0.6}Sn_{0.4}Br_3$ NPLs films under daylight and UV light. These films were fabricated by spray coating NPLs solution on different substrates (i.e., paper, fabric, wood, Cu, polyimide (PI), polyethylene terephthalate (PET), glass, silicon (Si) and leaf). Scale bar, 5 mm. h) Images of a stretchable film composed of HABr-passivated $MAPb_{0.6}Sn_{0.4}Br_3$ NPLs on the SEBS substrate under different degrees of stretch. Scale bar, 5 mm.

rapid crystal growth immediately after nucleation. The resulting NPLs exhibit pure blue emission, centered at 460 nm, with a narrow FWHM of 20 nm and a high PLQY of 87%. This approach overcomes the inherent instability of Sn-doped perovskites and the difficulty in preparing monodispersed ultrasmall NPLs. We demonstrated that use of bromide-containing organic cations (HABr) for surface passivation significantly increases both the PLQY and stability of NPL solution and films. The NPL films were fabricated using a convenient and scalable spray-coating method and were easily patterned. The superior performance and ease of processing properties of these NPLs suggest their substantial potential for future applications.

4. Experimental Section

Materials: Methylammonium bromide (MABr, 99%) was purchased from Dyesol. lead (II) bromide ($PbBr_2$, 99.99%), tin (II) bromide ($SnBr_2$, 99.99%), anhydrous N, N-dimethylformamide (DMF, 99.8%), oleic acid (OA, analytical reagent 90%), n-octylamine (OCT, 99%), n-butylammonium bromide (BABr, 98%), n-hexylammonium bromide (HABr, 98%), n-octylammonium bromide (OABr, 98%),

phenylammonium bromide (PhABr, 98%), benzylammonium bromide (BZABr, 98%), anhydrous toluene (99.8%) and acetonitrile (99.8%) were purchased from Sigma Aldrich. All chemicals were used as obtained, without further purification. Styrene-ethylene-butylene-styrene (SEBS) polymer was purchased from Kraton.

Synthesis of $MAPb_{1-x}Sn_xBr_3$ Perovskite NPLs: Initially, 0.2 mmol MABr, 0.2 mmol $PbBr_2$/$SnBr_2$ (in the desired molar ratio) and 2 mL DMF were loaded in a 10-mL vial and stirred until they had fully dissolved. Subsequently, 300 µL OA and 10 µL OCT were added at the same time and the mixture was stirred for 30 min to obtain the precursor solution. This 400 µL precursor solution was incrementally introduced into a temperature-regulated blend of 5 mL toluene and 10 µL OCT then stirred for 5 minutes. The obtained blue-emitting NPLs solution was precipitated by adding 5 mL of acetonitrile in a dropwise manner, followed by centrifugation at 12 000 rpm for 5 minutes. The resultant precipitate was then re-dispersed in toluene.

Passivation of $MAPb_{1-x}Sn_xBr_3$ Perovskite NPLs: Excess amounts of BABr, HABr, OABr, PhABr, and BZABr were combined with 20 mL toluene separately and stirred vigorously at 60 °C for 2 hours. The undissolved materials were separated by centrifugation. The supernatant was used to re-disperse the purified $MAPb_{1-x}Sn_xBr_3$ perovskite NPLs. Finally, the passivated $MAPb_{1-x}Sn_xBr_3$ perovskite NPLs solution was obtained by centrifuging at 12 000 rpm for 1 minute to eliminate the precipitate.

NPLs Film Deposition: A laser was utilized to pattern the spray mask. Prior to spray coating, the NPLs solution was centrifuged at 12 000 rpm for 1 min to remove the precipitate. Following this, the solution was transferred into an airbrush kit with a compressor (equipped with a 0.3 mm tip), to achieve a uniform blue-emitting pattern by spraying back and forth over a masked substrate.

Characterization: PL spectra of perovskite NPLs in solution and films were collected using an FP8500 spectrofluorometer (JASCO). The PLQYs of perovskite NPLs in solution and films were also measured by the FP8500 spectrofluorometer coupled to an integrating sphere (ILF-835). Time-resolved PL lifetimes were determined using FluoroTime 300 (PicoQuant) with a 405-nm pulsed laser. The absorption spectra were recorded employing a Lambda 465 UV–vis spectrophotometer (PerkinElmer). X-ray photoelectron spectra of perovskite NPLs were measured using a K-alpha instrument (Thermo Scientific™) with a monochromatic Al Kα radiation source (1486.6 eV). X-ray diffraction (XRD) patterns of the NPLs were collected using an AXS D8-Advance diffractometer (Bruker). Transmission electron microscopy (TEM) images were obtained using a JEM 2100F (JEOL) with an operating voltage of 200 kV. The surface morphologies of NPL films were measured using a field-emission scanning electron microscope (SEM, Merlin Compact, Zeiss). The thickness of the perovskite NPLs was assessed using an atomic force microscope (AFM, NX-10, Park systems). To prepare the sample for AFM analysis, the perovskite NPL solution was spin-coated at 6000 rpm for 1 minute onto a silicon substrate. The NPL solution was diluted more than 10 times to ensure the formation of discernible stacked NPL layers on the substrate. Scanning transmission electron microscopy (STEM) measurements were performed on an FEI Tecnai F20 microscope with an operating voltage of 200 kV. Contact angles of 10 µL droplets of NPL solution on various substrates were measured with an optical contact-angle meter (JC2000D).

Supporting Information

Supporting Information is available from the Wiley Online Library or from the author.

Acknowledgements

F.C. and K.Y.J. contributed equally to this work. This work was supported by the National Research Foundation of Korea (NRF) grant funded by the Korea government (Ministry of Science and ICT) (NRF-2016R1A3B1908431, 2022M3H4A1A04096380).

Conflict of Interest

The authors declare no conflict of interest.

Data Availability Statement

The data that support the findings of this study are available from the corresponding author upon reasonable request.

Keywords

films, HABr passivation, perovskite, stability, ultrasmall nanoplatelets

Received: February 5, 2024
Revised: June 10, 2024
Published online:

[1] J. S. Kim, J.-M. Heo, G.-S. Park, S.-J. Woo, C. Cho, H. J. Yun, D.-H. Kim, J. Park, S.-C. Lee, S.-H. Park, E. Yoon, N. C. Greenham, T.-W. Lee, *Nature* **2022**, *611*, 688.
[2] Y.-H. Kim, S. Kim, A. Kakekhani, J. Park, J. Park, Y.-H. Lee, H. Xu, S. Nagane, R. B. Wexler, D.-H. Kim, S. H. Jo, L. Martínez-Sarti, P. Tan, A. Sadhanala, G.-S. Park, Y.-W. Kim, B. Hu, H. J. Bolink, S. Yoo, R. H. Friend, A. M. Rappe, T.-W. Lee, *Nat. Photonics* **2021**, *15*, 148.
[3] Y. Zhao, K. Zhu, *Chem. Soc. Rev.* **2016**, *45*, 655.
[4] T.-H. Han, K. Y. Jang, Y. Dong, R. H. Friend, E. H. Sargent, T.-W. Lee, *Nat. Rev. Mater.* **2021**, *7*, 757.
[5] Z. Chu, W. Zhang, J. Jiang, Z. Qu, F. Ma, Y. Zhao, X. Chu, Y. Shen, Y. Li, Z. Yin, X. Zhang, J. You, *Nat. Electron.* **2023**, *6*, 360.
[6] A. Fakharuddin, M. K. Gangishetty, M. Abdi-Jalebi, S.-H. Chin, A. R. bin Mohd Yusoff, D. N. Congreve, W. Tress, F. Deschler, M. Vasilopoulou, H. J. Bolink, *Nat. Electron.* **2022**, *5*, 203.
[7] S. Peng, S. Wang, D. Zhao, X. Li, C. Liang, J. Xia, T. Zhang, G. Xing, Z. Tang, *Small Methods* **2019**, *3*, 1900196.
[8] M. Karlsson, Z. Yi, S. Reichert, X. Luo, W. Lin, Z. Zhang, C. Bao, R. Zhang, S. Bai, G. Zheng, P. Teng, L. Duan, Y. Lu, K. Zheng, T. Pullerits, C. Deibel, W. Xu, R. Friend, F. Gao, *Nat. Commun.* **2021**, *12*, 361.
[9] H. Wang, F. Ye, J. Sun, Z. Wang, C. Zhang, J. Qian, X. Zhang, W. C. H. Choy, X. W. Sun, K. Wang, W. Zhao, *ACS Energy Lett.* **2022**, *7*, 1137.
[10] C. Bi, Z. Yao, X. Sun, X. Wei, J. Wang, J. Tian, *Adv. Mater.* **2021**, *33*, 2006722.
[11] Y. Dong, Y.-K. Wang, F. Yuan, A. Johnston, Y. Liu, D. Ma, M.-J. Choi, B. Chen, M. Chekini, S.-W. Baek, L. K. Sagar, J. Fan, Y. Hou, M. Wu, S. Lee, B. Sun, S. Hoogland, R. Quintero-Bermudez, H. Ebe, P. Todorovic, F. Dinic, P. Li, H. T. Kung, M. I. Saidaminov, E. Kumacheva, E. Spiecker, L.-S. Liao, O. Voznyy, Z.-H. Lu, E. H. Sargent, *Nat. Nanotech.* **2020**, *15*, 668.
[12] A. Liu, C. Bi, J. Tian, *Adv. Funct. Mater.* **2022**, *32*, 2207069.
[13] Q. Chen, J. Wu, X. Ou, B. Huang, J. Almutlaq, A. A. Zhumekenov, X. Guan, S. Han, L. Liang, Z. Yi, J. Li, X. Xie, Y. Wang, Y. Li, D. Fan, D. B. L. Teh, A. H. All, O. F. Mohammed, O. M. Bakr, T. Wu, M. Bettinelli, H. Yang, W. Huang, X. Liu, *Nature* **2018**, *561*, 88.
[14] M. Worku, Y. Tian, C. Zhou, H. Lin, M. Chaaban, L.-j. Xu, Q. He, D. Beery, Y. Zhou, X. Lin, Y.-f. Su, Y. Xin, B. Ma, *Sci. Adv.* **2020**, *6*, eaaz5961.
[15] V. Malgras, J. Henzie, T. Takei, Y. Yamauchi, *Angew. Chem., Int. Ed.* **2018**, *130*, 9019.
[16] S. Wang, C. Bi, J. Yuan, L. Zhang, J. Tian, *ACS Energy Lett.* **2018**, *3*, 245.
[17] C. Bi, Z. Yao, J. Hu, X. Wang, M. Zhang, S. Tian, A. Liu, Y. Lu, N. H. de Leeuw, M. Sui, J. Tian, *ACS Energy Lett.* **2023**, *8*, 731.

[18] K. Zheng, Q. Zhu, M. Abdellah, M. E. Messing, W. Zhang, A. Generalov, Y. Niu, L. Ribaud, S. E. Canton, T. Pullerits, *J. Phys. Chem. Lett.* **2015**, *6*, 2969.
[19] M. Roy, Vikram, B., A. Alam, M. Aslam, *Phys. Chem. Chem. Phys.* **2021**, *23*, 27355.
[20] D. M. Jang, D. H. Kim, K. Park, J. Park, J. W. Lee, J. K. Song, *J Mater Chem* **2016**, *4*, 10625.
[21] H. M. Jang, S. H. Lee, K. Y. Jang, J. Park, T.-W. Lee, *Commun. Phys.* **2023**, *6*, 372.
[22] T.-W. Lee, S. H. Lee, Y.-H. Kim, H. Cho, US. 10109805B2, **2015**.
[23] C. Liang, H. Gu, Y. Xia, Z. Wang, X. Liu, J. Xia, S. Zuo, Y. Hu, X. Gao, W. Hui, L. Chao, T. Niu, M. Fang, H. Lu, H. Dong, H. Yu, S. Chen, X. Ran, L. Song, B. Li, J. Zhang, Y. Peng, G. Shao, J. Wang, Y. Chen, G. Xing, W. Huang, *Nat. Energy* **2021**, *6*, 38.
[24] K. Wang, Z.-Y. Lin, Z. Zhang, L. Jin, K. Ma, A. H. Coffey, H. R. Atapattu, Y. Gao, J. Y. Park, Z. Wei, B. P. Finkenauer, C. Zhu, X. Meng, S. N. Chowdhury, Z. Chen, T. Terlier, T.-H. Do, Y. Yao, K. R. Graham, A. Boltasseva, T.-F. Guo, L. Huang, H. Gao, B. M. Savoie, L. Dou, *Nat. Commun.* **2023**, *14*, 397.
[25] Y. Liu, J. Cui, K. Du, H. Tian, Z. He, Q. Zhou, Z. Yang, Y. Deng, D. Chen, X. Zuo, Y. Ren, L. Wang, H. Zhu, B. Zhao, D. Di, J. Wang, R. H. Friend, Y. Jin, *Nat. Photonics* **2019**, *13*, 760.
[26] J.-H. Yoo, S. Kim, H. Lee, C. Park, T.-W. Lee, J.-W. Park, *ACS Appl. Mater. Interfaces* **2023**, *15*, 39461.
[27] S.-W. Dai, B.-W. Hsu, C.-Y. Chen, C.-A. Lee, H.-Y. Liu, H.-F. Wang, Y.-C. Huang, T.-L. Wu, A. Manikandan, R.-M. Ho, C.-S. Tsao, C.-H. Cheng, Y.-L. Chueh, H.-W. Lin, *Adv. Mater.* **2018**, *30*, 1705532.
[28] F. Di Stasio, S. Christodoulou, N. Huo, G. Konstantatos, *Chem. Mater.* **2017**, *29*, 7663.
[29] Y. Kim, E. Yassitepe, O. Voznyy, R. Comin, G. Walters, X. Gong, P. Kanjanaboos, A. F. Nogueira, E. H. Sargent, *ACS Appl. Mater. Interfaces* **2015**, *7*, 25007.
[30] D. N. Minh, J. Kim, J. Hyon, J. H. Sim, H. H. Sowlih, C. Seo, J. Nam, S. Eom, S. Suk, S. Lee, E. Kim, Y. Kang, *Chem. Mater.* **2017**, *29*, 5713.
[31] J. C. Dahl, X. Wang, X. Huang, E. M. Chan, A. P. Alivisatos, *J. Am. Chem. Soc.* **2020**, *142*, 11915.
[32] Y. Bekenstein, B. A. Koscher, S. W. Eaton, P. Yang, A. P. Alivisatos, *J. Am. Chem. Soc.* **2015**, *137*, 16008.
[33] L. Dou, A. B. Wong, Y. Yu, M. Lai, N. Kornienko, S. W. Eaton, A. Fu, C. G. Bischak, J. Ma, T. Ding, N. S. Ginsberg, L.-W. Wang, A. P. Alivisatos, P. Yang, *Science* **2015**, *349*, 1518.
[34] J. Song, L. Xu, J. Li, J. Xue, Y. Dong, X. Li, H. Zeng, *Adv. Mater.* **2016**, *28*, 4861.
[35] A. Chakrabarty, S. Satija, U. Gangwar, S. Sapra, *Chem. Mater.* **2020**, *32*, 721.
[36] K.-L. Huang, Y.-H. Chang, P.-Y. Lin, K.-W. Hsu, D. E. Beck, S. Hsieh, *J. Phys. Chem. C* **2022**, *126*, 13441.
[37] N. Li, Z. Zhu, J. Li, A. K. Y. Jen, L. Wang, *Adv. Energy Mater.* **2018**, *8*, 1800525.
[38] S. Li, Z. Shi, F. Zhang, L. Wang, Z. Ma, D. Yang, Z. Yao, D. Wu, T.-T. Xu, Y. Tian, Y. Zhang, C. Shan, X. J. Li, *Chem. Mater.* **2019**, *31*, 3917.
[39] S. Das, A. De, A. Samanta, *J. Phys. Chem. Lett.* **2020**, *11*, 1178.
[40] D. Yan, Q. Mo, S. Zhao, W. Cai, Z. Zang, *Nanoscale* **2021**, *13*, 9740.
[41] A. Kirakosyan, N. D. Chinh, M. R. Sihn, M.-G. Jeon, J.-R. Jeong, D. Kim, J. H. Jang, J. Choi, *J. Phys. Chem. Lett.* **2019**, *10*, 4222.
[42] B. Tang, S. Wang, H. Liu, N. Mou, A. S. Portniagin, P. Chen, Y. Wu, X. Gao, D. Lei, A. L. Rogach, *Adv. Opt. Mater.* **2023**, *12*, 2301524.
[43] S. Jiang, Y. Song, H. Kang, B. Li, K. Yang, G. Xing, Y. Yu, S. Li, P. Zhao, T. Zhang, *ACS Appl. Mater. Interfaces* **2021**, *14*, 3385.